LANGMUIR Article
Cite This: Langmuir 2018, 34, 8499–8507
pubs.acs.org/Langmuir

Structural and Optical Investigations of Quasi-Single Crystal Eu^{3+}-Doped $BaWO_4$ Thin Films

Wen Deng,[†] Fengjun Chun,[†] Wen Li,[†] Hai Su,[†] Binbin Zhang,[†] Meilin Xie,[†] Haitao Zhang,[†] Xiang Chu,[†] Long Jin,[†] Chao Luo,[†] and Weiqing Yang*[,†,‡]

[†]Key Laboratory of Advanced Technologies of Materials (Ministry of Education), School of Materials Science and Engineering, and [‡]State Key Laboratory of Traction Power, Southwest Jiaotong University, Chengdu 610031, People's Republic of China

ABSTRACT: Scheelite-structure tungstates with unique structural features and excellent luminescence possess promising applications, such as light-emitting diodes (LEDs), scintillators, and displays. The controllable growth of high quality and uniform composition thin films mounted on cheap substrates is a key factor to realize the above commercial applications, however, which is also a big challenge due to the difficult stress release stemming from intrinsic lattice mismatches. Here, we employed the simple and composition-controlled polymer-assisted deposition (PAD) method to successfully obtain a series of high quality and well-proportioned $BaWO_4$:Eu^{3+} (BWOE) thin films with red emission. Screening out the unbound freedom metal ions by poly(ether imide) (PEI) and ethylene diamine tetraacetic acid (EDTA), the firmly bound metal ions (Ba^{2+}, W^{6+} and Eu^{3+}) in polymer solution were applied to accurately control the chemical composition and effectively governed the release of stress during the growth process of BWOE thin films. Furthermore, XRD, SEM and EDS mapping detections evidently authenticated the quasi-single crystallinity, uniform morphology and well-distributed composition of as-grown thin films. Additionally, excited by 250 nm light, these thin films could efficiently produce the red emission, peaked at around 612 nm originated from the $^5D_0 \rightarrow {}^7F_2$ transition of Eu^{3+}. Moreover, the optimal doping concentration of thin films was confirmed to be 9% and corresponding Commission International de l'Eclairage (CIE) chromaticity coordinate was (0.618, 0.365), which evidently implied the excellent color rending index. Therefore, this work highlights the rather superior PAD method to prepare uniform and high-quality BWOE thin films, which can be expanded toward the other photoelectric devices including white lighted-emitting diodes, scintillators, displays, and photoelectric detectors.

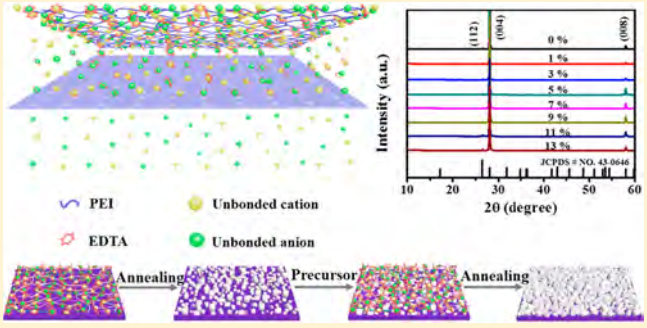

INTRODUCTION

As we know, the scheelite-structure tungstates with the unique structural features, excellent luminescence and other superior photoelectric properties present lots of potentially applicative prospects, such as light-emitting diodes (LEDs), scintillation detectors, and displays.[1,2] As a fascinating group of inorganic-functional materials, tungstates have attracted special attention because of their excellent chemical stability, high average refractive index and high X-ray absorption coefficient.[3] Generally, the scheelite-type tungstates with C_{4h} point group symmetry structure are MWO_4 (M = Ca, Sr, Ba, Pb), whose M^{2+} is surrounded by the adjacent eight oxygen ions constituting the aberrant cube, while W^{6+} is located in the center of tetrahedron of O^{2-} coming into being the WO_4^{2-} group.[4] Because of the unique structural features and the presence of allowed O^{2-} to W^{6+} transition, tungstates are regarded as the efficient host materials for luminescence systems. Besides, the entire visible spectrum decomposed in blue, green, and red components can be obtained due to the self-luminescence of scheelite-type tungstates.[5] Assigned to ligand-to-metal charge transfer (LMCT) transitions in the near-UV region, the self-emission intensity is too weak compared with commercialized luminescent materials.[5,6] Thus, it is urgent to introduce a luminescent center to enhance the emission intensity for the effective promotion of the practical lighting applications. Especially, owing to their high monochromaticity, long lifetime, high energy efficiency, and low resistance, rare earth (RE)-doped tungstates have been proven to be excellent luminescence materials.[7,8] As the luminescent center ions, the rare-earth ions, such as Sm^{3+}, Tb^{3+}, Er^{3+}, Eu^{3+}, and Pr^{3+}, are usually doped into tungstates with different microstructures.[9−12] For instance, Liao et al. reported the microspheric $CaWO_4$:Tb^{3+} green-phosphor originating from the $^5D_4 \rightarrow {}^7F_5$ transition of Tb^{3+} by regulating the RE ion-doped concentrations.[13] Singh's group synthesized the red lighting $BaWO_4$:Eu^{3+} nanophosphors by mechanical activation, and researched the optical properties from energy transfer dynamics and time-resolved photoluminescence.[7]

Received: May 8, 2018
Revised: June 19, 2018
Published: June 26, 2018

DOI: 10.1021/acs.langmuir.8b01499
Langmuir 2018, 34, 8499−8507

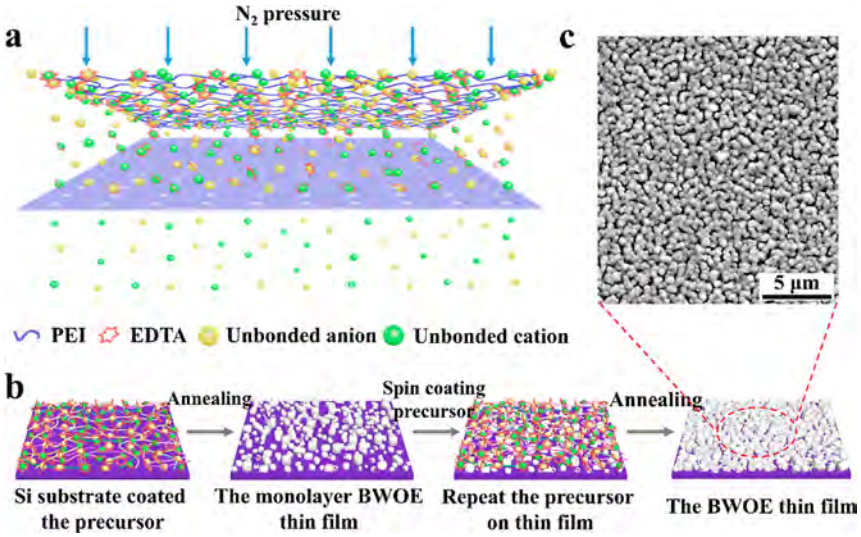

Figure 1. Schematic illustration for the preparation procedure of BWOE thin films. (a) The ultrafiltration model of preparation precursor. (b) Schematic illustration of the main processing steps. (c) SEM image of thin films under the optimum condition.

Koshy et al. studied the Eu-doped $BaWO_4$ thin films on structure and PL performance by pulsed laser deposition (PLD) technique.[14] However, the aforementioned phosphor powders cannot catch up with the luminescent thin films in some respects, such as low resistance, high uniformity, easy to be mounted on cheap substrates, mechanical stability, and superior resolution.[15,16]

Except for the above advantages of thin films, however, the introduction of RE ions increase the precise controlling problem of the multimetal elements. Moreover, the intrinsic and extrinsic stress release problems will directly lead to microstructural alteration, stratified and low-quality luminescent thin films during the growth and cooling processes, even seriously effecting the durability as well as the optical properties.[17] The above two kinds of stress are mainly generated by the accumulating effect of defects during deposition and the lattice mismatch or different thermal expansion coefficients between films and substrate materials, respectively.[17,18] Aiming at the stress of epitaxial Vanadium−Hydrogen (V−H) thin films, Gemma et al. researched discrete stress release cases via the rearrangement of pre-existing defects.[19] Also, Guerain et al. investigated the contribution of both destructive and nondestructive processes to stress release phenomena in α-Cr_2O_3 oxide thin films.[20] Even though they achieved some improvements, the challenging requirement of multimetal controllability and the stress release were yet to be fulfilled effectively. In this regard, a simple PAD technique touches down researchers minds. This method could not only precisely control the distribution of multimetal elements by binding the target ions with polymers, but also reduce the effect of stress release on film quality by arranging the bound ions to deposit in order.[21] Relying on the covalent bonding of polymers with metal ions, this method of preparing the solution has several advantages compared with traditional preparation methods, including (i) the long-term stability even storing several months, (ii) the ability to coat large areas, (iii) the growth of high quality and homogeneous epitaxial films, and (iv) suitable for almost all metal ions based on the viscosity.[22−24]

In this paper, we demonstrate a sequence high-quality and uniform distribution quasi-single crystallinity BOWE thin films, which is directly grown on the monocrystalline silicon substrates by the simple PAD method. The metal ions bound by PEI and EDTA were arranged on the substrate surface in order and stress release can be effectively controlled during the growth and cooling procedure of thin films. Furthermore, XRD, SEM, and EDS mapping detections evidently authenticated the quasi-single crystallinity, uniform morphology, and well-distributed composition of as-grown thin films. Additionally, the red emission spectrum peaked at around 612 nm, attributed to the $^5D_0 \rightarrow {}^7F_2$ transition of Eu^{3+}, could be effectively excited by the excitation light of 255 nm. Comparing the luminescence properties of different doping concentrations of Eu^{3+}, the concentration quench occurred at 9% in this BOWE thin films. Besides, the decay lifetime, annealing temperature and time are studied in detail. The CIE chromaticity coordinate is found to be (0.618, 0.365), indicating the excellent luminescence properties. Moreover, the as-prepared BWOE thin films not only emphasize the importance of PAD technique to obtain superior thin films, but also can be applied to other photoelectric devices.

EXPERIMENTAL SECTION

Materials. All of the chemicals were directly used as received without further purification, including poly(ether imide) (PEI, 99.99%, Aldrich), ethylene diamine tetraacetic acid (EDTA, 99.99%, Aladdin), europium chloride ($EuCl_3$, 99.99%, Aladdin), barium nitrate ($BaNO_3$, AR, Keshi), and chlorinated tungsten (WCl_6, AR, Keshi).

Preparation of Precursor Solution and Thin Films. A series of Eu^{3+}-doped BWO thin films were synthesized by PAD method. A total of 1 g PEI was dissolved in 40 mL of deionized water with continuous stirring at room temperature, and then 1 g EDTA was added slowly into the solution. After dissolved completely, 1 g $Ba(NO_3)_2$ was further dissolved into the obtained solution until the metal ions were bound effectively by PEI and EDTA. At this time, the as-prepared chelate solution was transferred into an ultrafiltration cup and filtered three times under the aegis of N_2. In the same way, W^{6+} and Eu^{3+} precursors were prepared, respectively. The ionic concentration, as-prepared precursors with 18.6364, 16.4767, and 13.523 g/L for Ba^{2+}, W^{6+}, and Eu^{3+}, respectively. Ba^{2+}, W^{6+}, and Eu^{3+} precursors were mixed with a certain stoichiometric proportion of $Ba^{2+}/W^{6+}/Eu^{3+}$ = 1:1:c, which kept the equal mole ratio of barium to tungsten and changed the mole concentration of Eu_c^{3+} (c = 0, 1, 3, 5,

DOI: 10.1021/acs.langmuir.8b01499
Langmuir 2018, 34, 8499−8507

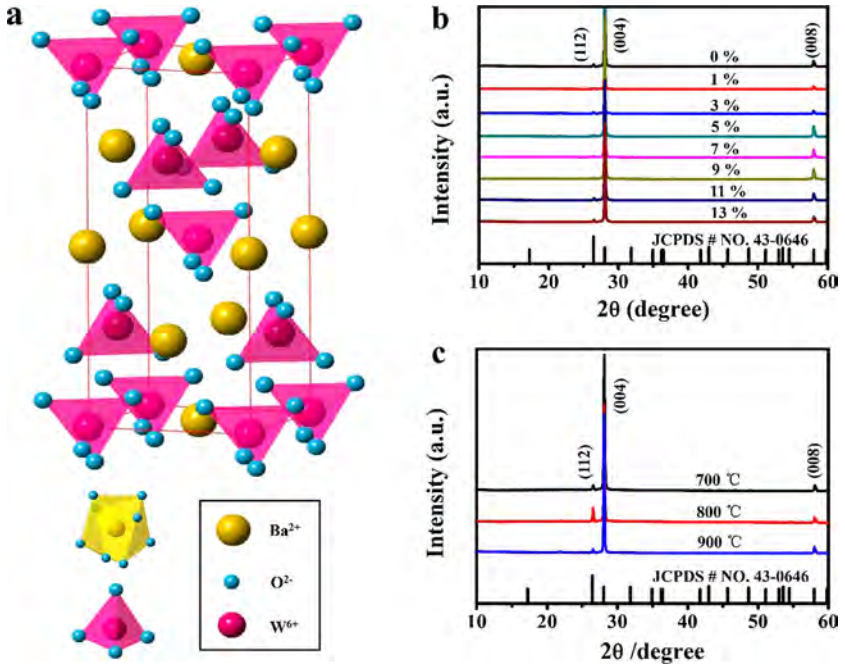

Figure 2. Structure characterization of BWOE thin films. (a) The drawn schematic view of $BaWO_4$ crystal structure, (b) XRD patterns of BWO thin films with different Eu^{3+} doped concentration (c = 0−13%), and (c) annealing temperature.

7, 9, 11, and 13%). The as-prepared precursor solution was spin-coated onto silicon substrate at 2000 rpm for 30 s, respectively, then annealed with different temperature to induce cross-linking. According to the need of film thickness, several precursor layers were coated on the silicon substrates.

Characterization. The ion concentrations of as-prepared precursors were detected by inductively coupled plasma-atomic emission spectroscopy (ICP). The crystal structural characterization and phase identification of the samples were carried out by the X Pert Pro (Holland) X-ray diffract meter with Cu Kα1 radiation (λ = 0.15406 nm) from 5° to 60°. Surface morphology and particle size distribution of the thin films were investigated by a FEI QUANTA FEG 250 scanning electron microscope (SEM) and energy-dispersive X-ray spectroscopy (EDX, S4800), respectively. The photoluminescence spectra, excitation spectra and decay times were examined by FLS980 (Edinburgh Instruments) spectrometer with a 450 W xenon lamp at room temperature.

RESULTS AND DISCUSSION

PEI and EDTA were elaborately chosen as the chelating agent to bind target metal ions and the corresponding filtration-model schematic illustration of as-prepared precursor was obviously shown in Figure 1a. During the preparation of precursors, EDTA not only actively bound the metal ions to ensure a homogeneous distribution, but also offered the combination of hydrogen bonding and electrostatic attraction with PEI.[21,24,25] The firm-bound metal ions by PEI and EDTA could not got through the filter membrane while the other unbound metal ions and some small organic molecules would be percolated under the pressure of N_2.[21] So, we obtained the uniform as-prepared precursor including firmly bound metal ions (Ba^{2+}, W^{6+}, Eu^{3+}). And then, as the processes shown in Figure 1b, a series of high quality and well-proportioned BWOE thin films were prepared with different conditions.

According to the atomic concatenate forms and structure data of BWO,[26,27] the drawn schematic view of BWO model showed in Figure 2a. When the Eu^{3+} ions were doped into BWO, the Eu^{3+} would occupy the position of Ba^{2+}. Because $EuWO_4$ and $BaWO_4$ had the same crystal structure, which caused that Eu^{3+} could replace the Ba^{2+} and formed the high-efficiency luminescent center.[28] And uncertain distortion came into being around the octahedron, which is attributed to the different atomic radius between Ba^{2+} and Eu^{3+}. First, the effect of different doping concentrations on crystal structural under fixed 6 layers were studied. The effect of Eu^{3+}doped concentrations (0−13%) on the XRD patterns of the thin films shown in Figure 2b. It could be seen that the high crystallinity of the samples were demonstrated by the strong diffraction peaks, and that all the peaks matched well with the standard data of scheelite phase BWO (JCPDS card No. 43−0646). The main diffraction peaks at 28.054°, 58.017° as well as the negligible peak at 26.450° corresponding to (004), (008), and (112) plane, respectively, obviously demonstrated the quasi-single crystal BWOE thin films grown along the main plane (00k).[29,30] Such high quality thin films on common substrate with intrinsic lattice mismatches mainly attributed to the effective stress release of polymer firm-binding metal ions.[31,32] On the other hand, there are no traces of additional peaks from other phases including the RE ions. The unalloyed and doped thin films have the same diffraction directions, which indicates that the Eu^{3+} ions have been doped into the host lattice of BWO effectively.[33] Besides, the doping concentration at 9% has the strongest diffraction intensity, which laterally means the best crystallinity at 9%. In order to improve the growth conditions of BWOE thin films, we also studied the XRD of BWOE thin films annealed at different temperature. Figure 2c confirms that the same diffraction peaks are revealed at 26.450°, 28.054°, and 58.017° with different temperature, which is consistent with the results of Figure 2b. However, as we can see, there are several peaks missing compared with the JCPDS. The main reason for this phenomenon is that preferred growth orientations on the (100) silicon substrate, which are dominated by the total free energy variation during the growth process, and the minimization of the surface, interface, and strain energies

DOI: 10.1021/acs.langmuir.8b01499
Langmuir 2018, 34, 8499−8507

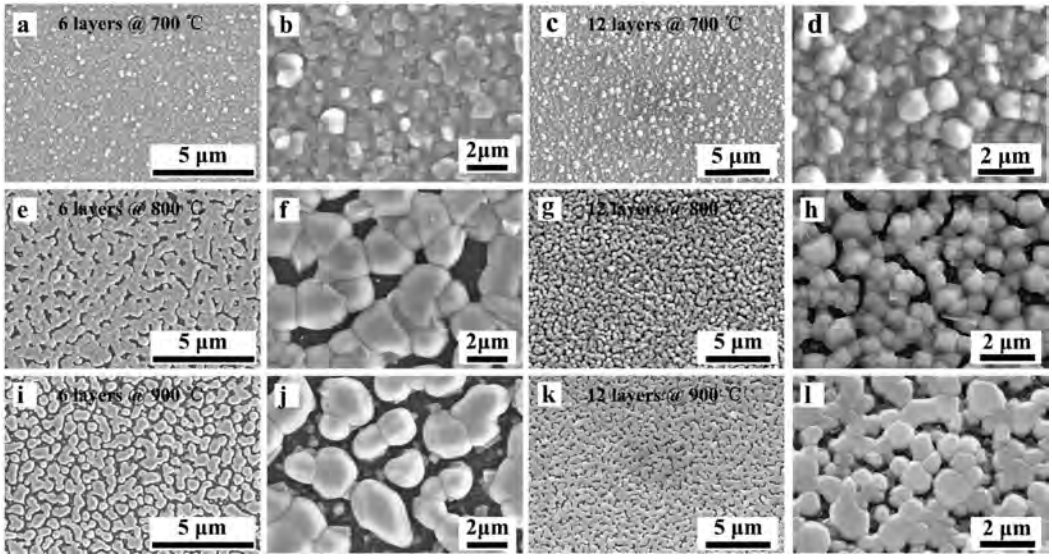

Figure 3. SEM images of BWOE thin films with different layers and annealing temperature: (a, b), (e, f), (i, j) 6 layers and (c, d), (g, h), (k, l) 12 layers for 700, 800, and 900 °C, severally.

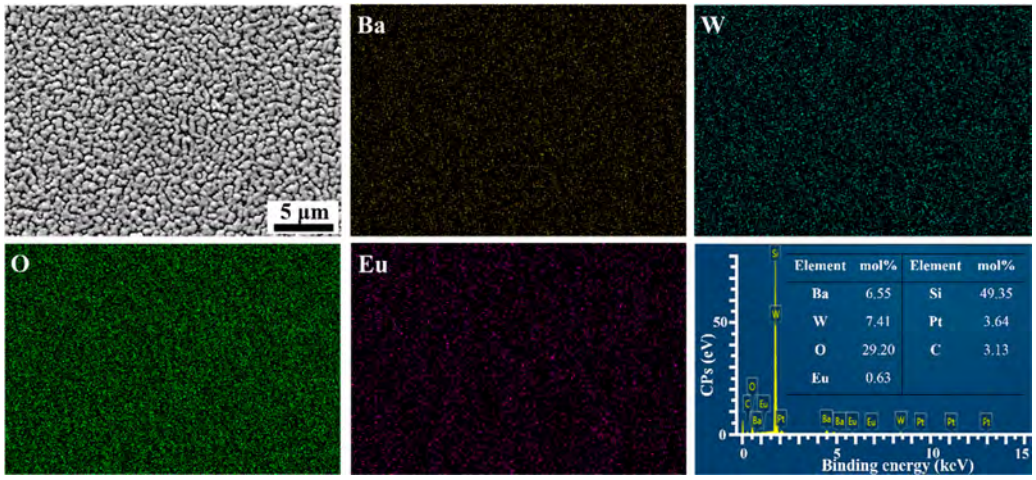

Figure 4. Elemental mapping of BWOE thin films at c = 9%.

between different oriented grains controlled the driving force of the thin film grains growth. Therefore, under the control of macromolecular assistance and driving force, the epitaxial film grew along the favorable crystal surface, thus obtaining the BWOE films with the type of quasi-single crystal.

In order to get insight into the microstructure of as-grown thin films, SEM measurement was employed to study the microgrowth mechanism with different synthesized temperature and layers. Fixed the concentration of Eu^{3+} at 9%, BWOE thin films with selected 6 layers and 12 layers were prepared at the annealing temperature of 700−900 °C and the corresponding SEM images were shown in Figure 3. The microscopy of BWOE thin films with 700 °C looks like some irregular sheets. With the increase of the annealing temperature, the average size of the BWOE gradually increases and their profile progressively become clear. The corresponding average size at 800 and 900 °C are about 0.41 and 0.46 μm, respectively. Moreover, the best crystallinity and homogeneity are reflected for 800 °C. The higher annealing temperature usually attributed to higher mobility of growth species on the substrate surface, which explained why the compactness with higher temperature could not catch up with that of 700 °C.[25] When the amount of layer increased to 12 layers, the additional layers of precursor solution filled in the porous structure and improved the compactness of thin films. As shown in Figure 3c,d,g,h,k,l, the tightness of all the samples were enhanced and the profiles became clear with the average size 0.23, 0.62, and 0.69 μm for 700−900 °C, respectively. Furthermore, as shown in Figure 4, the EDS-mapping of the BWOE thin film evidently presents that the elements evenly disperse in the films, which reveals that the PAD method can effectively control the homogeneity of multielements thin films.

For the in-depth analysis of luminescent behavior, we made a comprehensive study of emission spectra of as-prepared BWOE thin films with various Eu^{3+}-doped concentration from 0% to 13%. As shown in Figure 5a, the red emission spectra with the similar shapes should mainly ascribe to the intrinsic 4f−4f ($^5D_0 \rightarrow {}^7F_x$) transition of doped Eu^{3+} ions.[3,34,35] Furthermore, the emission peaks at 578, 592, 612, 654, and 702 nm are assigned to $^5D_0 \rightarrow {}^7F_0$, $^5D_0 \rightarrow {}^7F_1$, $^5D_0 \rightarrow {}^7F_2$, $^5D_0 \rightarrow {}^7F_3$, and $^5D_0 \rightarrow {}^7F_4$ transitions of Eu^{3+}, respectively. Among them, the ascendant red emission at 612 nm shows up a good

DOI: 10.1021/acs.langmuir.8b01499
Langmuir 2018, 34, 8499−8507

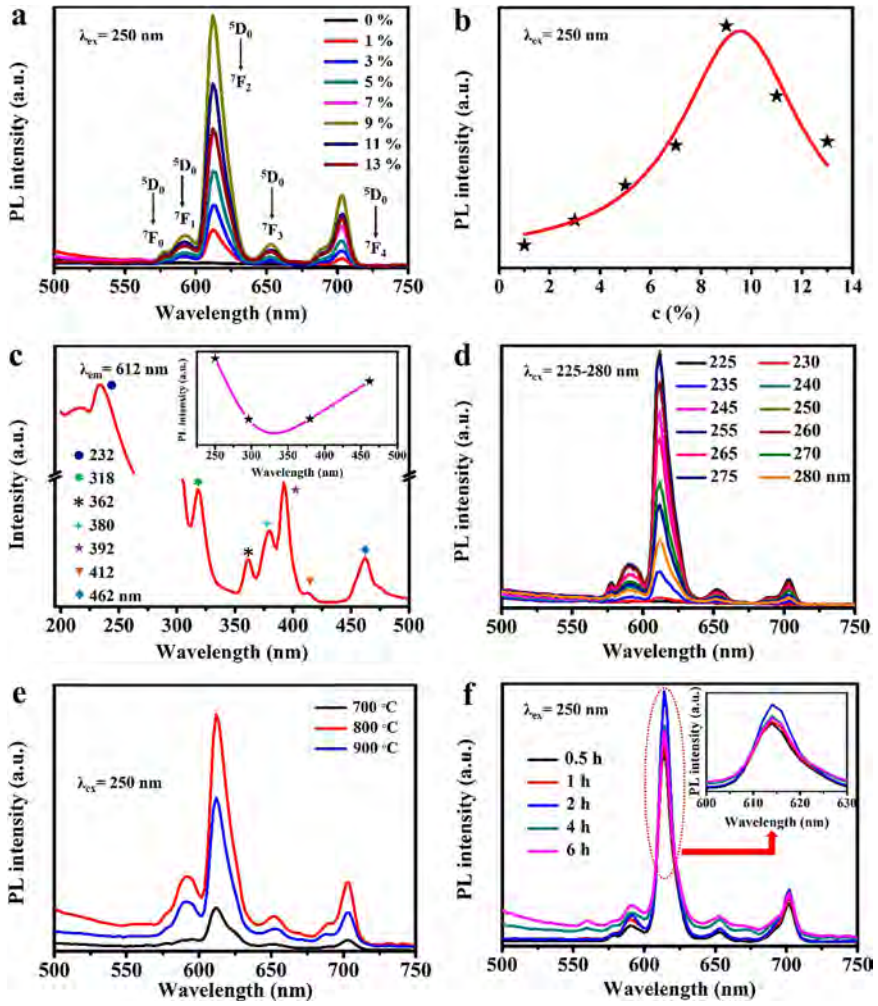

Figure 5. Luminescent properties of prepared BWOE thin films. (a) The emission spectra of BWOE thin films with different concentration of Eu^{3+} monitored at 250 nm. (b) The intensity comparison of Eu^{3+} doped BWOE concentration ranging from 0 to 13%. (c) Excitation spectra of as-prepared thin films monitored at 250 nm and corresponding PL intensity comparison of peak values in the inset. (d) Emission spectra with different excitation wavelength (λ_{ex} = 225−280 nm). (e) Emission spectra of BWOE thin films annealed at 700−900 °C. (f) The influence of annealing time on the luminescence properties.

color rendering index comparing with BWO powders doped with Eu^{3+} prepared by the solid state reaction and soft chemistry method.[36,37] As far as we know, the electric dipole transition gives rise to the $^5D_0 \rightarrow {}^7F_2$ line.[38] The position of Eu^{3+} in BWO has an effect on the luminescence intensity of the $^5D_0 \rightarrow {}^7F_2$ (612 nm) electronic transition. Moreover, its intensity dramatically increase when the luminescence center Eu^{3+} take up a low-symmetry local site which introduces a strong electric field to drive the transition.[35,39] However, the $^5D_0 \rightarrow {}^7F_1$ transition caused by the magnetic dipole transition is corresponding to a site of inversion symmetry. Hence, as stated above, the Eu^{3+} ions in our work locate at a site of noninversion symmetry and then emit red luminescence.

Besides, it was found that the luminescence intensity gradually increased with increasing the Eu^{3+} concentration from 1%, and then it reached a maximum as the Eu^{3+} concentration at 9% composition, as exhibited in Figure 5a,b. However, the luminescence intensity started to decrease with further increasing the concentration. This kind of unique luminescent intensity changing trend of first increased and then decreased with the increase of doping concentration, is intrinsically attributed to the concentration quenching.[40] Specifically, with the low concentration ranging from 1% to 9%, the average distance of Eu^{3+} ions were large enough to avoid the interaction of the nearby Eu^{3+} ions.[41,42] In this case, the Eu^{3+} doped into the host crystal of BWO could effectively come into being the luminescence center. Nevertheless, when the doped concentration surpasses the extremity, the deformation force of lattice distortion would gradually become too weak to stimulate the electron to get through the valence band and enter the stable metastable state of the forbidden band.[40] Thus, luminescence intensity steadily decreased. In addition, the optimum quenching concentration was corresponding to the optimum property and the critical distance between the nearest Eu^{3+} ions. It was perfectly consistent with the Figure 2b. With the increase of Eu^{3+} doping concentration, the shorter distance of Eu^{3+} and the easier formation of crystal defect made the nonradiation transition chance augment.[41] So the decreased number of photons reduced the luminescence performance.

The excitation spectra of BWOE thin films were collected by pumping the emission wavelength at 612 nm, shown in Figure 5c. The excitation spectra with a broad charge transfer (CT) banded from 224 to 284 nm was broke at 9−300 k in vertical

DOI: 10.1021/acs.langmuir.8b01499
Langmuir 2018, 34, 8499−8507

Table 1. Comparisons of BWOE Thin Films Prepared by PAD and Previous Reports

materials	method	microstructure	temp	time	fwhm	ref
BWO film	CE	nonuniform	RT		>80 nm	43
BWOE powder		nonuniform	700 °C	4 h	>15 nm	26
BWOE film	PLD	nonuniform	800 °C	4 h		14
BWOE film	RFMS	uniform	1500 °C	5 h	<10 nm	16
BWOE film	PAD	uniform	800 °C	2 h	15 nm	this work

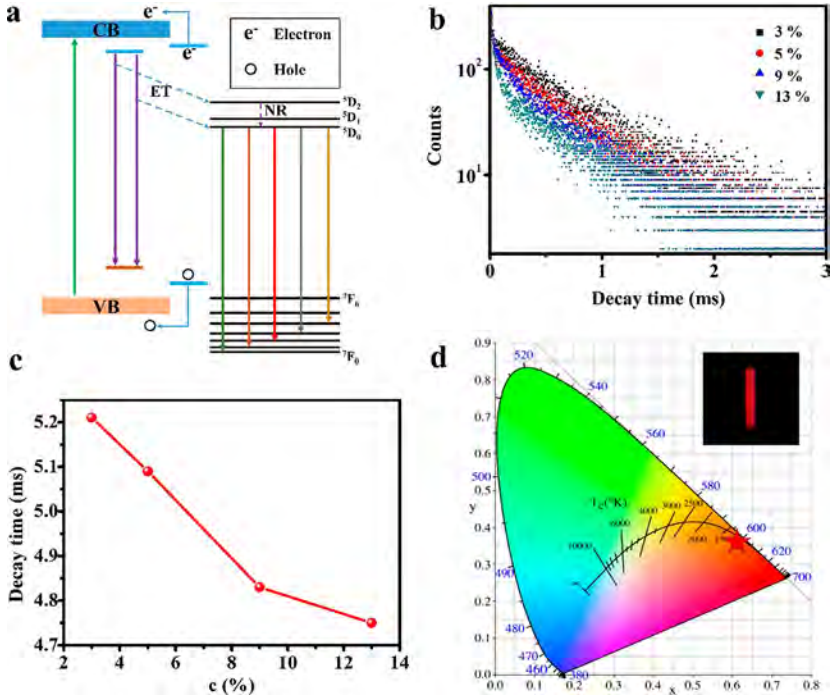

Figure 6. (a) Energy transition mechanism of Eu^{3+} in $BaWO_4$ matrix. (b) Decay curves of thin films with different doped concentrations, (c) average decay time trace, and (d) CIE diagram of thin films monitored at 612 nm.

coordinates and had a maximum intensity at 232 nm and some characteristic excitation peaks. These peaks could be attributed to the intraconfigurational (f–f) transitions of Eu^{3+}, as shown at 318 nm ($^7F_0 \rightarrow {}^5H_3$), 362 nm ($^7F_0 \rightarrow {}^5D_4$), 380 nm ($^7F_0 \rightarrow {}^5L_7$), 392 nm ($^7F_0 \rightarrow {}^5L_6$), 412 nm ($^7F_0 \rightarrow {}^5D_3$), and 462 nm ($^7F_0 \rightarrow {}^5D_2$).[7] However, these excitation transitions could not obtain the most efficient luminescence properties, except for the excitation wavelength at 250 nm in the UV region. The inset of Figure 5c was the photoluminescence (PL) intensities comparison of 250 nm with other characteristic excitation peaks. With the excited wavelength increased from 250 to 462 nm, the luminescent properties decreased and then improved, which demonstrated that 250 nm was the best excitation transition. To consolidate the result, we further discussed the effect of the CT region on optical properties. The emission spectrum excited by 225 to 280 nm was shown in Figure 5d. The intensity of the curves with the same shapes rapidly increased with increasing the wavelength of excitation light source and had a maximum intensity pumped by 250 nm. More importantly, these peaks of emission spectra excited by a series of various light did not any slightly shift, which evidently revealed the complete validness of the above excited light.

For the systematical investigation on the effect of annealing temperature and time on the luminescent properties, we employed the BWOE thin films with fixing Eu^{3+}-doped concentration at 9%. As displayed in Figure 5e, it was easily found that the maximum PL intensity was obtained at 800 °C, which was 5.44× and 1.54× than that of 700 and 900 °C, respectively. Additionally, we further studied the impact of annealing time on luminescence properties from 0.5 to 6 h at the fixed annealing temperature of 800 °C. It was obviously shown that the PL intensity appeared at a peak value at 2 h in Figure 5f and the inset. We speculated that the reaction time might be too short to accomplish the nucleation completely, which led to the inferior optical performance. Unfortunately, when the annealing time was too long, the increasing particle size reduced due to the boundary scattering, so the PL intensity slightly decreased. However, it is interesting to note that the as-prepared BWOE thin films by PAD method have special advantages over by other methods in uniformity, synthesis temperature, and annealing time. To point it out, herein the comparison is presented from the materials, synthetic method, microstructure, annealing temperature, heat treatment time, and PL spectrum full width at half-maximum (fwhm), as shown in Table 1. Here, CE, PLD, RFMS, and PAD stand for the cell electrochemical, pulsed laser deposition, radio frequency magnetron sputtering, and polymer-assisted deposition technique, respectively.

For a deep insight into the luminescent mechanism of as-grown BWOE thin films, Figure 6a clearly schematizes the energy transition process between BWO and Eu^{3+}. As a result, the thin films could be excited to excitation state by the CT energy transition of WO_4^{2-} group. When the thin films were excited, the excited electrons of WO_4^{2-} group could move

DOI: 10.1021/acs.langmuir.8b01499
Langmuir 2018, 34, 8499–8507

from the ground 2p states of O^{2-} to excitation 5d states of W^{6+}.[44] At the same time, the holes broke away from the constraint of O^{2-} and entered into the valence band. When the recombination of holes and electrons occurred, the induced CT transferred the energy to Eu^{3+}, which induced the characteristic emission from $^5D_0$ to ^7F_J(J = 0, 1, 2, 3, 4), then the red emission of Eu^{3+} generated.[28]

Besides, we investigated the decay lifetimes of BWOE thin films for revealing the luminescent dynamics with λ_{ex} = 250 nm and λ_{em} = 612 nm, shown in Figure 6b. The double exponential decay eq 1 was made to fit the decay behavior:

$$I = A_1 e^{-t/\tau_1} + A_2 e^{-t/\tau_2} \quad (1)$$

$$\tau = (A_1\tau_1^2 + A_2\tau_2^2)/(A_1\tau_1 + A_2\tau_2) \quad (2)$$

Equation 2 was used for calculating the average lifetime. While in eq 1, I was the PL intensity; A_1 and A_2 were the constants; τ_1 and τ_2 were the rapid decay and slow decay components, respectively. On the basis of eqs 1 and 2, the fitting results of τ_1, τ_2, A_1, A_2, and τ* are listed in Figure 6c and Table 2. The average decay times were calculated to be 5.22, 5.09, 4.83, and 4.75 ms for BWOE samples with different doping concentrations (c = 3%, 5%, 9%, 13%, respectively), presenting a decrease trend for gradually raising the concentration of Eu^{3+} due to the concentration quenching mentioned above and fluorescence resonance energy transfer (FRET).[45] It is an important factor for Eu^{3+} locating at or near the surface of BWO during the FRET process. Because when the concentration of Eu^{3+} increased, the energy immigration or interaction strengthens and the number of effectively doped ions into the crystal decreased. In addition, the nonequivalent substitutions would produce positive charge defects in order to keep charge balance, which led to nonradiative relaxation and then reduced the decay times.[46]

Table 2. Decay Lifetimes of BWOE Thin Films

samples	τ_1	τ_2	A_1	A_2	τ* (ms)
c = 3%	4.76	573.52	1325.03	110.41	5.22
c = 5%	4.90	552.17	1203.34	126.16	5.09
c = 9%	62.15	586.12	227.59	98.63	4.83
c = 13%	13.17	602.54	689.54	54.65	4.75

To investigate the color properties of BWOE thin films under 250 nm excitation, the CIE in 1931 was used for explore its color rending index. As shown in Figure 6d, it is found that the color coordinates of BWOE are calculated to be (0.618, 0.365) and its inset of Figure 6d shows the red emission of thin films excited by the rectangular UV light, which possesses excellent red color rendering index and a potential applications for LEDs.

CONCLUSIONS

In summary, the red lighting $BaWO_4$:Eu_c^{3+} (c = 0−13%) thin films with high-quality are synthesized by the PAD method to effectively address the difficult problem of the multimetal controllability and the harsh effect of stress release on film quality. PEI as well as EDTA are proved to bind the metal ions and precisely control the uniform distribution of elements. Moreover, the XRD, SEM and EDS mapping results reflect the quasi-single crystallinity, the superior morphology and homogeneity of thin films. Additionally, the emission spectra of as-prepared thin films is composed of a sharp PL peak at 612 nm with an full width at half-maximum about 13 nm, produced by the $^5D_0 \rightarrow {}^7F_2$ transition of Eu^{3+} ions. Furthermore, the optimal doping concentration of Eu^{3+} is authenticated to be 9%. The optimal preparation condition are 800 °C for 2 h and the corresponding CIE chromaticity coordinates (0.618, 0.365) that sheds light on promising application for white light. Besides, the energy transition mechanism of Eu^{3+} in $BaWO_4$ matrix and luminescence kinetics are discussed in detail. This work highlights the rather superior PAD technique to prepare uniform and high-quality $BaWO_4$:Eu^{3+} thin films. We believe that this kind of unique high quality quasi-single crystallinity thin films will be a promising functional materials for the w-LEDs for solid state light, scintillators, displays, and photoelectric detectors.

AUTHOR INFORMATION

Corresponding Author

*E-mail: wqyang@swjtu.edu.cn.

ORCID

Weiqing Yang: 0000-0001-8828-9862

Author Contributions

W.D. performed all the experiments and manuscript. F.J.C. and W.L. contributed to part of the luminescence properties evaluation, and H.S., B.B.Z., X.C., M.L.X., L.J., and C.L. contributed to the material characterizations. W.D., F.J.C., W.L., H.S., H.T.Z., and W.Q.Y. analyzed the data and composed the manuscript. H.T.Z. and W.Q.Y. planned the study and supervised the project. All authors discussed the results and commented on the manuscript.

Notes

The authors declare no competing financial interest.

ACKNOWLEDGMENTS

Thanks for the help from the Analytical and Testing Center of Southwest Jiaotong University. This work is support by the National Natural Science Foundation of China (No. 51602265), the Independent Research Project of State Key Laboratory of Traction Power (Nos. 2017TPL_Z04 and 2016TPL_Z03), the Fundamental Research Funds for the Central Universities of China (Nos. 2682016ZY01, 2682017ZDPY01, 2682016CX074, and 2682017CY06) and China Postdoctoral Science Foundation (No. 2016M592692).

REFERENCES

(1) Ju, Z. H.; Wei, R. P.; Ma, J. X.; Pang, C. R.; Liu, W. S. A Novel Orange Emissive Phosphor $SrWO_4$: Sm^{3+} for White Light-emitting Diodes. *J. Alloys Compd.* **2010**, *507*, 133−136.

(2) Liao, J.; Qiu, B.; Wen, H.; Chen, J.; You, W.; Liu, L. Synthesis Process and Luminescence Properties of Tm^{3+} in AWO_4 (A = Ca, Sr, Ba) Blue Phosphors. *J. Alloys Compd.* **2009**, *487*, 758−762.

(3) Yang, W.; Qu, Y.; Pan, K.; Wang, G.; Li, Y. Enhanced Photoelectric Conversion Efficiency of Dye Sensitized Solar Cells via the Incorporation of One Dimensional Luminescent $BaWO_4$: Eu^{3+} Nanowires. *Chem. Commun.* **2016**, *52*, 11124−11126.

(4) Dabre, K. V.; Dhoble, S. L.; Lochab, J. Synthesis and Luminescence Properties of Ce^{3+} Doped MWO_4 (M = Ca, Sr and Ba) Microcrystalline Phosphors. *J. Lumin.* **2014**, *149*, 348−352.

(5) Shivakumara, C.; Saraf, R.; Behera, S.; Dhananjaya, N.; Nagabhushana, H. Scheelite-type MWO_4 (M = Ca, Sr, and Ba) Nanophosphors: Facile Synthesis, Structural Characterization, Photoluminescence and Photocatalytic Properties. *Mater. Res. Bull.* **2015**, *61*, 422−432.

(6) Barbosa, H. P.; Kai, J.; Silva, I. G. N.; Rodrigues, L. C. V.; Felinto, M. C. F. C.; Hölsä, J.; Brito, H. F.; et al. Luminescence

DOI: 10.1021/acs.langmuir.8b01499
Langmuir 2018, 34, 8499−8507

Investigation of R^{3+}-doped Alkaline Earth Tungstates Prepared by a Soft Chemistry Method. *J. Lumin.* **2016**, *170*, 736−742.
(7) Jena, P.; Gupta, S. K.; Verma, N. K.; Singh, A. K.; Kadam, R. M. Energy Transfer Dynamics and Time Resolved Photoluminescence in $BaWO_4$: Eu^{3+} Nanophosphors Synthesized by Mechanical Activation. *New J. Chem.* **2017**, *41*, 8947−8958.
(8) Lin, J.; Zeng, Z.; Ma, Q.; Wang, Q.; Zhang, Y. Effects of Multiple Irradiations on Luminescent Materials and Energy Savings-A Case Study for the Synthesis of $BaMO_4$: Ln^{3+} (M = W, Mo; Ln = Eu, Tb) Phosphors. *Energy* **2014**, *64*, 551−556.
(9) Lin, C. K.; Yu, M.; Pang, M. L.; Lin, J. Photoluminescent Properties of Sol-gel Derived (La, Gd) MgB_5O_{10}: Ce^{3+}/Tb^{3+} Nanocrystalline Thin Films. *Opt. Mater.* **2006**, *28*, 913−918.
(10) Lee, M. J.; Park, S. H.; Song, Y. H.; Ji, E. K.; Humayoun, U. B.; Lee, D. B.; Yoon, D. H. Fabrication of Phosphor Ceramic Plate Using Green-emitting $Lu_3Al_5O_{12}$: Ce^{3+} phosphor for high power LEDs. *Mater. Lett.* **2015**, *161*, 708−711.
(11) Cai, G. M.; Yang, N.; Liu, H. X.; Si, J. Y.; Zhang, Y. Q. Single-phased and Color Tunable $LiSrBO_3$: Dy^{3+}, Tm^{3+}, Eu^{3+} Phosphors for White-light-emitting Application. *J. Lumin.* **2017**, *187*, 211−220.
(12) Zhang, L.; Pan, H.; Liu, H.; Zhang, B. B.; Jin, L.; Zhu, M. H.; Yang, W. Q. Theoretical Spectra Identification and Fluorescent Properties of Reddish Orange Sm-doped $BaTiO_3$ Phosphors. *J. Alloys Compd.* **2015**, *643*, 247−252.
(13) Liao, J.; Qiu, B.; Wen, H.; You, W. Photoluminescence Green in Microspheres of $CaWO_4$: Tb^{3+} Processed in Conventional Hydrothermal. *Opt. Mater.* **2009**, *31*, 1513−1516.
(14) Pillai, N. V.; Pillai, V. P. M.; Vinodkumar, R.; Navas, I.; Ganesan, V.; Koshy, P. Influence of Europium Oxide Doping on the Structural and Optical Properties of Pulsed Laser Ablated Barium Tungstate Thin Films. *J. Alloys Compd.* **2011**, *509*, 2745−2752.
(15) Kominami, H.; Yamasaki, T.; Nakanishi, Y.; Hara, K. Study of Crystallization Process of Eu Doped $SrGa_2S_4$ Thin Film Phosphors by Two Electron Beams Evaporation and 355 nm Nd: YAG Laser-annealing. *J. Lumin.* **2012**, *132*, 3100−3102.
(16) Cho, S. Annealing Effect on Properties of $BaWO_4$:Eu^{3+} Phosphor Thin Films Grown on Glass Substrates by Radio-frequency Magnetron Sputtering. *Appl. Surf. Sci.* **2018**, *432*, 202−206.
(17) Ning, H.; Liu, X.; Zhang, H.; Fang, Z.; Cai, W.; Chen, J.; Zhang, Z.; et al. Effect of Intrinsic Stress on Structural and Optical Properties of Amorphous Si-doped SnO_2 Thin-film. *Materials* **2017**, *10*, 24−31.
(18) Wagner, S.; Kramer, T.; Uchida, H.; Dobron, P.; Cizek, J.; Pundt, A. Mechanical Stress and Stress Release Channels in 10−350 nm Palladium Hydrogen Thin Films with Different Micro-structures. *Acta Mater.* **2016**, *114*, 116−125.
(19) Gemma, R.; Dobron, P.; Cizek, J.; Pundt, A. Stress Release and Defect Occurrence in $V_{1-x}Fe_x$ Films Upon Hydrogen Loading: H-induced Superabundant Vacancies, Movement and Creation of Dislocations. *Acta Mater.* **2014**, *67*, 308−323.
(20) Guerain, M.; Rakotovao, F.; Brou, S. Y.; Bonnet, G.; Panicaud, B.; Grosseau, J. L.; Goudeau, P. Stress Release in α-Cr_2O_3 Oxide Thin Films Formed on Ni30-Cr and Fe47-Cr Alloys. *J. Alloys Compd.* **2017**, *718*, 223−230.
(21) McCleskey, T. M.; Shi, P.; Bauer, E.; Highland, M. J.; Eastman, J. A.; Bi, Z. X.; Jia, Q. X.; et al. Nucleation and Growth of Epitaxial Metal-Oxide Films Based on Polymer-Assisted Deposition. *Chem. Soc. Rev.* **2014**, *43*, 2141−2146.
(22) Yi, Q.; Wu, J.; Zhao, J.; Wang, H.; Hu, J.; Dai, X.; Zou, G. Tuning Bandgap of p-type $Cu_2Zn(Sn, Ge)(S, Se)_4$ Semiconductor Thin Films via Aqueous Polymer-assisted Deposition. *ACS Appl. Mater. Interfaces* **2017**, *9*, 1602−1608.
(23) Yang, H.; Giri, A.; Moon, S.; Shin, S.; Myoung, J. M.; Jeong, U. Highly Scalable Synthesis of MoS_2 Thin Films with Precise Thickness Control via Polymer-assisted Deposition. *Chem. Mater.* **2017**, *29*, 5772−5776.
(24) Kim, Y. Y.; Hwang, J. S.; Kim, J. K.; Kumar, S.; Kim, J.; Kim, K. B.; Lee, J. M. Electrical and Optical Properties of Hydrogen Plasma Treated Molybdenum-doped Indium Oxide Films Synthesized by Polymer-assisted Deposition method. *Ceram. Int.* **2017**, *43*, S506−S510.
(25) Breckenfeld, E.; Kim, H.; Gorzkowski, E. P.; Sutto, T. E.; Piqué, A. Laser-processing of VO_2 Thin Films Synthesized by Polymer-assisted-deposition. *Appl. Surf. Sci.* **2017**, *397*, 152−158.
(26) Barros, B. S.; Lima, A. C.; Silva, Z. R.; Melo, D. M. A.; Alves, S. Synthesis and Photoluminescent Behavior of Eu^{3+}-doped Alkaline-earth Tungstates. *J. Phys. Chem. Solids* **2012**, *73*, 635−640.
(27) Cao, R.; Xu, H.; Peng, D.; Gou, Q.; Zhou, S.; Liu, P.; Yu, X. Synthesis and Luminescence Properties of $BaWO_4$: Sm^{3+}, Mo^{6+}/K^+ Red Phosphor. *J. Mater. Sci.: Mater. Electron.* **2015**, *26*, 6776−6780.
(28) Kang, F. W.; Hu, Y. H.; Chen, L.; Wang, X. J.; Wu, H. Y.; Mu, Z. F. Luminescent Properties of Eu^{3+} in MWO_4 (M = Ca, Sr, Ba) Matrix. *J. Lumin.* **2013**, *135*, 113−119.
(29) Ma, D.; Ye, Z.; Wang, L.; Huang, J.; Zhao, B. Deposition and Characteristics of CdO Films with Absolutely (200)-preferred Orientation. *Mater. Lett.* **2004**, *58*, 128−131.
(30) Tu, D.; Xu, C. N.; Fu, Y. Intense Red Emitting Mechanoluminescence from CaZnOS: Mn, Li with *c*-axis Preferred Orientation. *J. Adv. Dielectr.* **2014**, *4*, 1450017.
(31) Lim, H. J.; Kang, S. Y.; Hwang, C. S.; Kim, H. J. Analysis of Stresses in Ru Thin Flms Prepared by Chemical Vapor Deposition. *J. Vac. Sci. Technol., A* **2003**, *21*, 1381−1385.
(32) Enriquez, E.; Zhang, Y.; Chen, A.; Bi, Z.; Wang, Y.; Fu, E.; Jia, Q.; et al. Epitaxial Growth and Physical Properties of Ternary Nitride Thin Films by Polymer-assisted Deposition. *Appl. Phys. Lett.* **2016**, *109*, 081907.
(33) Tian, X.; Jiang, G.; Chen, Y.; Yin, M. Eu^{3+}, Li^+ Doped $CaWO_4$ Nanorods: Synthesis, Emission-decay Curves and Effective-refractive Index. *Curr. Appl. Phys.* **2014**, *14*, 1612−1615.
(34) Yang, W. Q.; Liu, H. G.; Gao, M.; Bai, Y.; Zhao, J. T.; Xu, X. D.; Lin, Y.; et al. Dual-luminescence-center Single-component White-light $Sr_2V_2O_7$: Eu^{3+} Phosphors for White LEDs. *Acta Mater.* **2013**, *61*, 5096−5104.
(35) Meza, O.; Villabona, E. G.; Diaz, L. A.; Desirena, H.; Rodriguez, J. L.; Perez, E. Luminescence Concentration Quenching Mechanism in Gd_2O_3: Eu^{3+}. *J. Phys. Chem. A* **2014**, *118*, 1390−1396.
(36) Bouzidi, C.; Ferhi, M.; Elhouichet, H.; Ferid, M. Spectroscopic Properties of Rare-earth (Eu^{3+}, Sm^{3+}) Doped $BaWO_4$ Powders. *J. Lumin.* **2015**, *161*, 448−455.
(37) Wang, R.; Liu, C.; Zeng, J.; Li, K.; Wang, H. Fabrication and Morphology Control of $BaWO_4$ Thin Films by Microwave Assisted Chemical Bath Deposition. *J. Solid State Chem.* **2009**, *182*, 677−684.
(38) Chen, G.; Wang, F.; Ji, W.; Liu, Y.; Zhang, X. Improved Luminescence of $CaWO_4$: Eu^{3+} Microspheres by Codoping Gd^{3+}. *Superlattices Microstruct.* **2016**, *90*, 30−37.
(39) Cheng, X.; Yuan, C.; Su, L.; Wang, Y.; Zhu, X. Effects of Pressure on the Emission of $CaWO_4$: Eu^{3+} Phosphor. *Opt. Mater.* **2014**, *37*, 214−217.
(40) Ju, G.; Hu, Y.; Chen, L.; Wang, X.; Mu, Z. Concentration Quenching of Persistent Luminescence. *Phys. B* **2013**, *415*, 1−4.
(41) Chun, F. J.; Zhang, B. B.; Su, H.; Osman, H.; Deng, W.; Deng, W. L.; Yang, W. Q.; et al. Preparation and Luminescent Properties of Self-organized Broccoli-like $SrMoO_4$: Pr^{3+} Superparticles. *J. Lumin.* **2017**, *190*, 69−75.
(42) Wu, B.; Yang, W.; Liu, H.; Huang, L.; Zhao, B.; Wang, C.; Lin, Y.; et al. Fluorescence Spectra and Crystal Field Analysis of $BaMoO_4$: Eu^{3+} Phosphors for White light-emitting Diodes. *Spectrochim. Acta, Part A* **2014**, *123*, 12−17.
(43) Chen, L. P.; Gao, Y. H.; Zhu, J. L. Luminescent Properties of $BaWO_4$ Films Prepared by Cell Electrochemical Technique. *Mater. Lett.* **2008**, *62*, 3434−3436.
(44) Du, P.; Wu, S.; Yu, J. S. Synthesis, Electronic Structure and Luminescence Properties of Color-controllable Dy^{3+}/Eu^{3+}-codoped $CaWO_4$ Phosphors. *J. Lumin.* **2016**, *173*, 192−198.
(45) Tu, D.; Liu, L.; Ju, Q.; Liu, Y. S.; Zhu, H. M.; Li, R. F.; Chen, X. Y. Time-resolved FRET Biosensor Based on Amine-functionalized Lanthanide-doped $NaYF_4$ Nanocrystals. *Angew. Chem., Int. Ed.* **2011**, *50*, 6306−6310.

DOI: 10.1021/acs.langmuir.8b01499
Langmuir 2018, 34, 8499−8507

(46) Wang, L.; Noh, H. M.; Moon, B. K.; Park, S. H.; Kim, K. H.; Shi, J.; Jeong, J. H. Dual-mode Luminescence with Broad Near UV and Blue Excitation Band from Sr_2CaMoO_6: Sm^{3+} Phosphor for White LEDs. *J. Phys. Chem. C* **2015**, *119*, 15517−15525.

DOI: 10.1021/acs.langmuir.8b01499
Langmuir 2018, 34, 8499−8507